Geophys. J. Int. (2000) **142,** 27–36

Signature of remnant slabs in the North Pacific from *P*-wave tomography

A. Gorbatov,[1,*] S. Widiyantoro,[1,†] Y. Fukao[1] and E. Gordeev[2]

[1] *Earthquake Research Institute, University of Tokyo, Yayoi* 1-1-1, *Bunkyo-ku, Tokyo* 113–0032, *Japan. E-mail: alexei@eri.u-tokyo.ac.jp*
[2] *Geophysical Survey of Russia, Piip Avenue* 9, *Petropavlovsk-Kamchatsky,* 683006, *Russia*

Accepted 2000 January 11. Received in original form 1999 August 15

SUMMARY

A 3-D ray-tracing technique was used in a global tomographic inversion in order to obtain tomographic images of the North Pacific. The data reported by the Geophysical Survey of Russia (1955–1997) were used together with the catalogues of the International Seismological Center (1964–1991) and the US Geological Survey National Earthquake Information Center (1991–1998), and the recompiled catalogue was reprocessed. The final data set, used for following the inversion, contained 523 430 summary ray paths. The whole of the Earth's mantle was parametrized by cells of $2^\circ \times 2^\circ$ and 19 layers. The large and sparse system of observation equations was solved using an iterative LSQR algorithm.

A subhorizontal high-velocity anomaly is revealed just above the 660 km discontinuity beneath the Aleutian subduction zone. This high-velocity feature is observed at latitudes of up to $\sim 70^\circ$N and is interpreted as a remnant of the subducted Kula plate, which disappeared through ridge subduction at about 48 Ma. A further positive velocity perturbation feature can be identified beneath the Chukotka peninsula and Okhotsk Sea, extending from ~ 300 to ~ 660 km depth and then either extending further down to ~ 800 km (Chukotka) or deflecting along the 660 km discontinuity (Okhotsk Sea). This high-velocity anomaly is interpreted as a remnant slab of the Okhotsk plate accreted to Siberia at ~ 55 Ma.

Key words: geodynamics, plate tectonics, ray tracing, seismic tomography, subduction.

1 INTRODUCTION

Since the pioneering work of Aki & Lee (1976), seismic tomography has become a powerful tool in probing the Earth's structure and tectonic processes. Global traveltime tomography was attempted first for the lower mantle by Dziewonski *et al.* (1977), and then for the whole mantle by Inoue *et al.* (1990). The recent tomographic inversions for the whole of the Earth's mantle, for example by Fukao *et al.* (1992) and Bijwaard *et al.* (1998), which attempt to close the gap between regional and global traveltime tomography, have revealed connections between deep mantle structures and contemporary tectonic processes. Many of such global or semi-global scale tomographic studies focus on the Northwest Pacific region (e.g. Zhou & Clayton 1990; Van der Hilst *et al.* 1991, 1993; Fukao *et al.* 1992; Van der Hilst *et al.* 1997). These studies also reveal the configurations of subducted slabs and their possible relation to tectonic histories. However, most of these studies focus on the subduction zones to the south of the Kurile arc ($< \sim 50^\circ$N). The subduction zones further to the north, Kurile–Kamchatka and Aleutian, are generally excluded from detailed analyses of tomographic images. To date, only a few tomographic studies have been performed for the Aleutian arc (e.g. Engdahl & Gubbins 1987; Widiyantoro 1997) and for the Kamchatka arc (e.g. Gorbatov *et al.* 1999). All these studies concentrate on the velocity anomalies associated with the Wadati–Benioff zones. They do not discuss the velocity anomalies further backarc, mainly because of the limited spatial coverage of traveltime data and the resulting lack of resolution. In an attempt to overcome this difficulty, we have collected as many arrival time data as possible from the observatories of the Geophysical Survey of Russia. We will incorporate these data into a global tomography in the hope of refining our understanding of tectonic processes in the North Pacific.

2 DATA

Fig. 1 shows the distribution of the 204 stations of the Geophysical Survey of Russia (GSR) used in our analysis. The

* Now at: Research School of Earth Sciences, the Australian National University, Canberra ACT 0200, Australia. E-mail: alexei@rses.anu.edu.au
† Institut Teknologi Bandung, Jl. Ganesa 10, Bandung 40132, Indonesia.

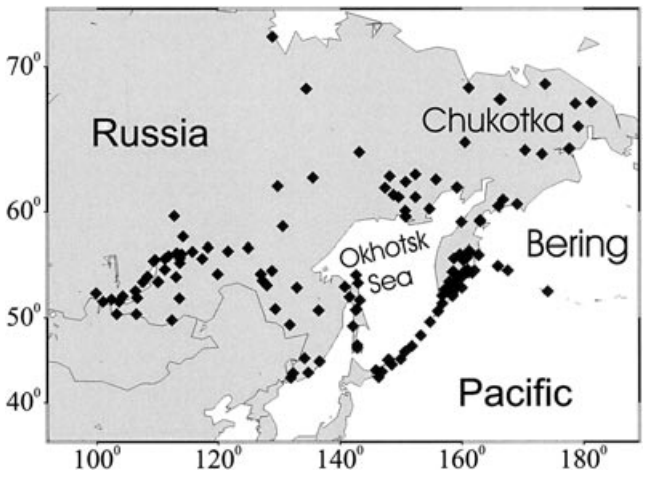

Figure 1. Distribution of the seismic stations (solid diamonds) included in the catalogue of the Geophysical Survey of Russia and used in our analysis.

P-wave arrival time data from these stations (1955–1997) were added to the catalogues of the International Seismological Center (ISC) (1964–1994) and the US Geological Survey National Earthquake Information Center (NEIC) (1995–1998). We then reprocessed the combined data set, which includes events and arrival times not reported in the ISC and NEIC catalogues. The ak135 (Kennett *et al.* 1995) earth reference model was perturbed by 2 per cent in the mantle and 10 per cent in the crust during hypocentral redetermination, and the events with epicentral dislocations greater than 25 km were removed from the data set. Finally, the hypocentres were redetermined using the ak135 velocity model for the earthquakes not relocated by Engdahl *et al.* (1998). For the earthquakes that were relocated by Engdahl *et al.* (1998) we adopted the hypocentral parameters given therein, which are considered to be sufficiently reliable because of the extensive reprocessing procedure using *P*, *S*, *PkiKP*, *PKPdf*, and the teleseismic depth phases *pP*, *pwP* and *sP* in the relocation. All data were corrected for the Earth's ellipticity and station elevations.

The use of summary rays reduces the effect of uneven sampling of structure by ray paths and the computational time required for ray tracing. Consequently, following the work of Van der Hilst *et al.* (1997), we combined the information from event clusters in a $1^\circ \times 1^\circ \times 50$ km volume and stations in a $1^\circ \times 1^\circ$ region into a single summary ray path. The residual time assigned to the summary ray was the median of all the data selected for that summary ray. Only ray paths with residuals smaller than 5 s and distances less than 95° were used. Each summary ray was composed of at least three individual rays. The final data set used for the inversion contained 523 430 summary ray paths.

3 METHOD

3.1 3-D ray tracing

We determine the regional and global structure simultaneously in order to minimize contamination of our regional model by heterogeneities located elsewhere. For this purpose, relatively small cells of $2^\circ \times 2^\circ$ and 19 layers, as used by Van der Hilst *et al.* (1997), were adopted to parametrize the whole Earth. The ak135 earth model (Kennett *et al.* 1995) was selected as a reference earth model. The accurate computation of traveltimes and ray paths in a heterogeneous earth is important in the tomographic inversions. Numerous recent local tomographic studies use 3-D ray tracing in order to achieve accurate ray-path calculations (e.g. Thurber 1983; Zhao *et al.* 1992; Mikumo *et al.* 1995); however, 3-D ray tracing is not commonly applied to regional or global traveltime tomography. In our whole-mantle tomography we, for the first time, implement the 3-D pseudo-bending ray-tracing method developed by Koketsu & Sekine (1998) for a spherical earth. This method was chosen because of its accurate and fast algorithm for calculating ray paths over large distances (Koketsu & Sekine 1998). The bending of a ray should be sensitive to the 3-D velocity structures surrounding the nominal ray path. The pseudo-bending method searches iteratively for the minimum traveltime ray path connecting the source and receiver, based on a three-point perturbation with a straight-line approximation of a ray-path segment. The difference between the calculated traveltimes for the 1-D and our 3-D ray-tracing techniques was found to be less than 0.1 s at a distance of 85° for several 1-D earth models. We believe that this difference reflects a reasonable agreement between the two totally different mathematical approaches to the tracing. Koketsu & Sekine (1998) give a detailed discussion about 3-D ray tracing for more complex media. Here, some discussion and brief comparisons of the results of 1-D and 3-D ray-tracing tomographic techniques using a common data set will be presented in the next subsection.

We used the LSQR algorithm of Page & Saunders (1982), implemented in seismic tomography for the first time by Nolet (1990), with the inclusion of event relocation, to solve the large and sparse system of observation equations. The velocity structure and hypocentral parameters were solved simultaneously in each iteration. The sum of the slowness vector in the previous iteration and the one in the new iterations was minimized in a least-squares sense to damp the solution towards the reference ak135 model. The roughness (gradient) of the solution was also minimized. Three iterations were performed. The root-mean-square (RMS) of the arrival time residuals calculated for the initial velocity model was 1.808 s. The RMS residuals after the first, second, and third iterations were 1.324, 1.165, and 1.127 s, respectively. The RMS improvement was 0.038 s between the second and third iterations, and the resulting image did not change visually. Therefore, the result of the third iteration was considered as the final one. This decision was reinforced by taking into account that the data kernel generation is somewhat time-consuming: one iteration took about five days (523 430 summary ray paths) on a SUN ULTRA 10 machine. Fig. 2 shows a map view of the final result, relative to ak135, for four depth ranges between 300 and 820 km in the North Pacific.

3.2 Comparison with 1-D ray tracing

The 3-D ray-tracing iterative technique has been applied only infrequently to tomographic inversion on a global scale. We discuss briefly the consequence of the application of 3-D ray tracing to a global-scale tomography. For comparison, we

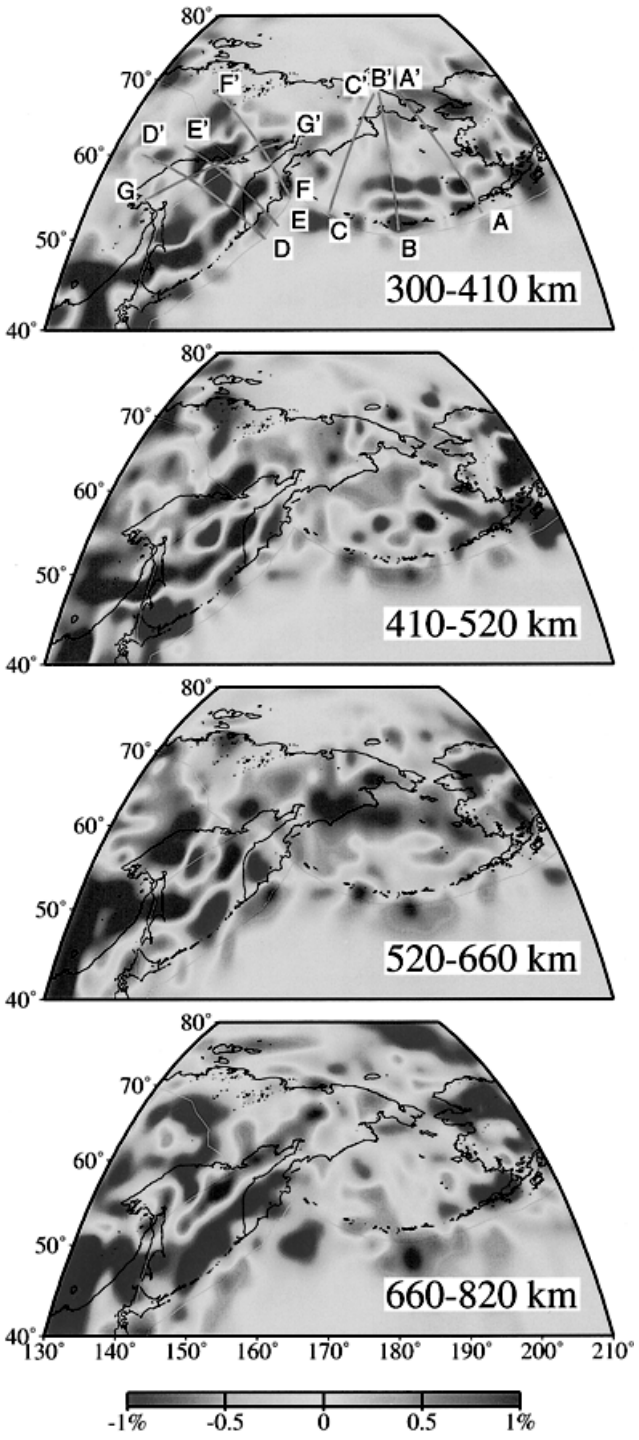

Figure 2. Results of *P*-wave tomographic inversion. Red and blue denote slow and fast velocity anomalies, respectively, with a scale in per cent relative to the reference model ak135 (Kennett *et al.* 1995). Green lines with letters at their ends mark the locations of the profiles that appear in Figs 5 and 7.

applied the iterative tomographic inversion scheme using 1-D ray tracing to the data set used in our study, using the same parametrization and inversion parameters as in the inversion using 3-D ray tracing. The 3-D velocity model obtained at each iteration was spherically averaged and the 1-D ray tracing was performed using this spherically averaged model for the subsequent iteration. Three iterations were performed. Fig. 3 is a comparison of the results from the 3-D and 1-D ray-tracing techniques (Figs 3a and 3b, respectively). Both techniques show the NE–SW-trending fast anomaly belt with similar values of perturbations at depths of 660–820 km behind the Kamchatka arc. The major difference is in the sharpness of images: the result of the 3-D ray tracing delineates the fast anomaly belt more sharply than the result of the 1-D ray tracing. This feature may be explained by the nature of 3-D ray tracing. Actual rays tend to propagate preferentially through a high-velocity zone located close to their nominal ray paths. Rays therefore tend to bend towards the high-velocity zone, resulting in a sharper image of the structure than in the 1-D ray tracing. Such ray bending does not occur in the 1-D ray tracing, resulting in a more diffuse image of the structure.

The RMS value of the traveltime residuals with respect to the final model was obtained as 1.29 s using 1-D ray tracing and as 1.12 s using 3-D ray tracing. A detailed comparison of the results of 3-D and 1-D ray-tracing tomographic techniques will be presented elsewhere.

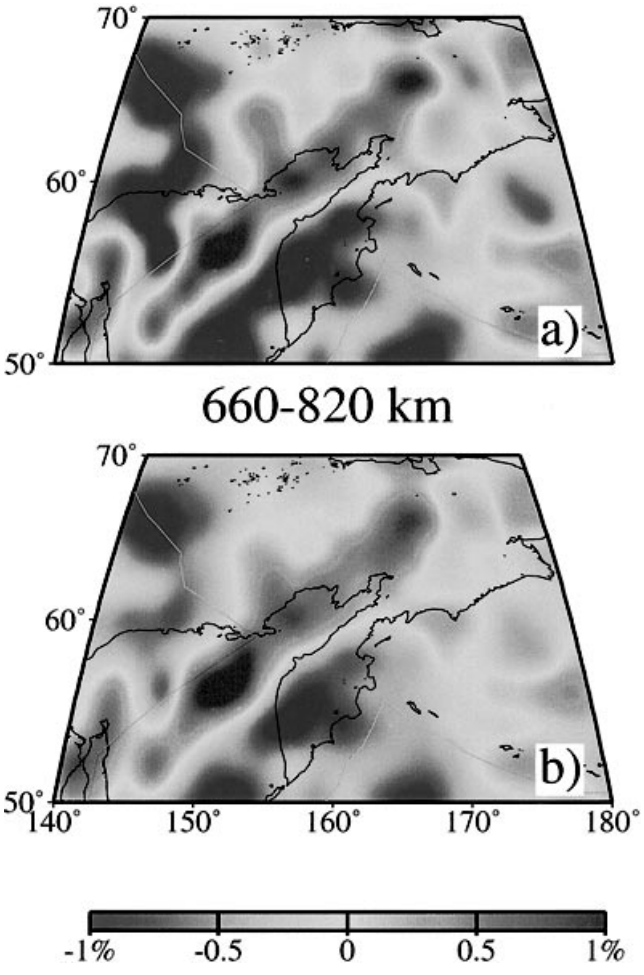

Figure 3. Comparison of the results obtained from the inversions with (a) 3-D and (b) 1-D ray-tracing techniques for the layer 660–820 km. The image obtained from 3-D ray tracing is sharper than that obtained from 1-D ray tracing.

3.3 Resolution

It is not feasible to calculate the resolution and covariance matrices because of the large matrix size. Consequently, the chequerboard resolution test (Spakman & Nolet 1988; Humphreys & Clayton 1988) was used. In this method, positive (3 per cent) and negative (−3 per cent) velocity perturbations were assigned to the 3-D blocks in order to make a chequerboard. These blocks were separated by a constant space in order to investigate possible smearing in the tomographic

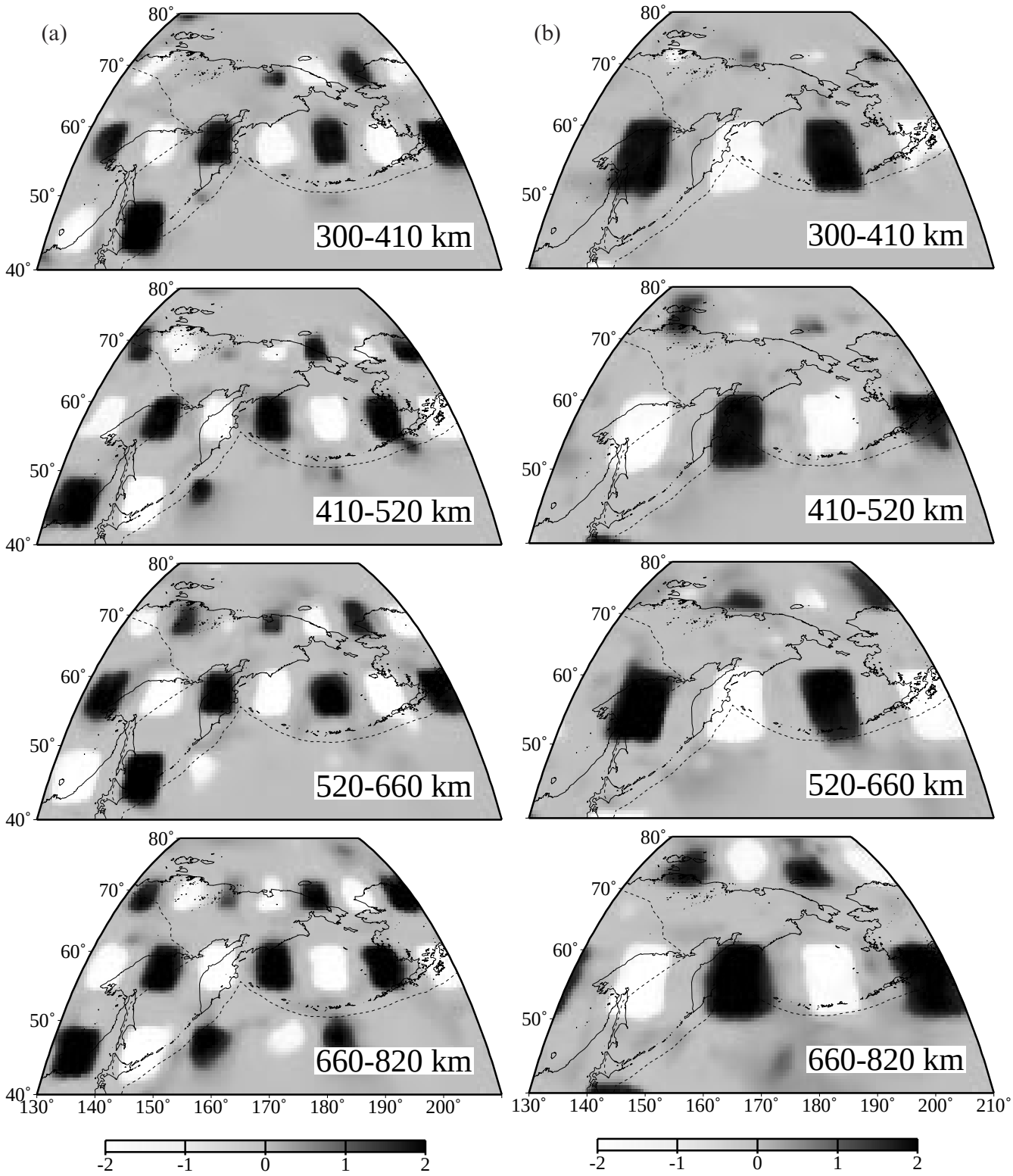

Figure 4. Results of the chequerboard resolution test for the zone of study. The blocks are of (a) $6^\circ \times 6^\circ$ and (b) $10^\circ \times 10^\circ$. The scale in per cent relative to the reference model is shown at the bottom.

images. It has been shown by Lévêque *et al.* (1993), however, that a small-scale resolution, implied by a synthetic test with small-scale anomalies, does not guarantee resolution on larger scales. Therefore, two patterns of $6^\circ \times 6^\circ$ and $10^\circ \times 10^\circ$ were constructed. Next, the synthetic arrival times were calculated using 3-D ray tracing in the chequerboard models. A random error with a standard deviation of 1 s was added to the synthetic data in order to simulate errors contained in the real data set. The same inversion technique with the same parameters as those used for tomographic imaging with the real data was applied to the synthetic data.

The results of the chequerboard tests are presented in Fig. 4, and show reasonably good recoveries (i.e. the pattern is clearly visible) of both the smaller and larger test patterns (4a and 4b) at and behind the island arcs. The resolution is generally poor further back on the Arctic Ocean and Pacific Ocean sides.

4 DEEP HIGH-VELOCITY ANOMALIES BEHIND THE ALEUTIAN AND KAMCHATKA ARCS

In the present paper we are mainly interested in the positive velocity perturbations behind the Aleutian and Kamchatka–Kurile arcs which might be related to the subducted slabs in the geological past. Fig. 2 shows the presence of a prominent high-velocity zone spreading far behind the Aleutian arc at depths of ~600 km beneath the Bering Sea in the area defined by ~60°N, ~70°N, ~165°E and ~190°E. In order to illuminate this high-velocity zone, cross-sectional images of the model are shown in Fig. 5 across the eastern, central and western Aleutian arc along profiles AA′, BB′ and CC′ (see Fig. 2 for location). The hypocentral distribution of earthquakes with magnitudes greater than 5.5 in the period 1964–1995 within a band of 50 km on both sides of the section plane is superposed on each cross-section.

Along profile AA′ (eastern Aleutian), the Wadati–Benioff zone extends down to a depth of about 150 km. The high-velocity zone associated with it extends further down, to about 400 km. Along profile BB′ (central Aleutian), the leading edge of the Wadati–Benioff zone reaches a depth of about 300 km, and the associated high-velocity anomaly extends down to depths below 400 km, as noted by Engdahl & Gubbins (1987). Thus the slab-related anomaly extends well beyond the leading edge of the Wadati–Benioff zone across both the eastern and central Aleutian arc. There is, however, a large gap between this slab-related anomaly and the high-velocity anomaly spreading extensively above the 600 km discontinuity beneath the Bering Sea. Checkerboard resolution tests (Fig. 4) indicate that this gap is a resolvable feature.

The Wadati–Benioff zone is poorly developed in the western Aleutian arc, and correspondingly the cross-section along profile CC′ does not show a slab-related fast anomaly at intermediate depths. In this cross-section, once more, a high-velocity zone flattens just above the 660 km discontinuity, showing a wide horizontal spread; it is well separated from the high-velocity zone associated with the presently subducting slab.

We performed an additional test, known as the restore resolution test, to examine to what extent continuous structures in the cross-sections are resolvable features. In the present study we are interested in the structures that may represent subducted slabs; therefore, a synthetic model depicting the subducted slabs is created. The hypothetical slabs are constructed

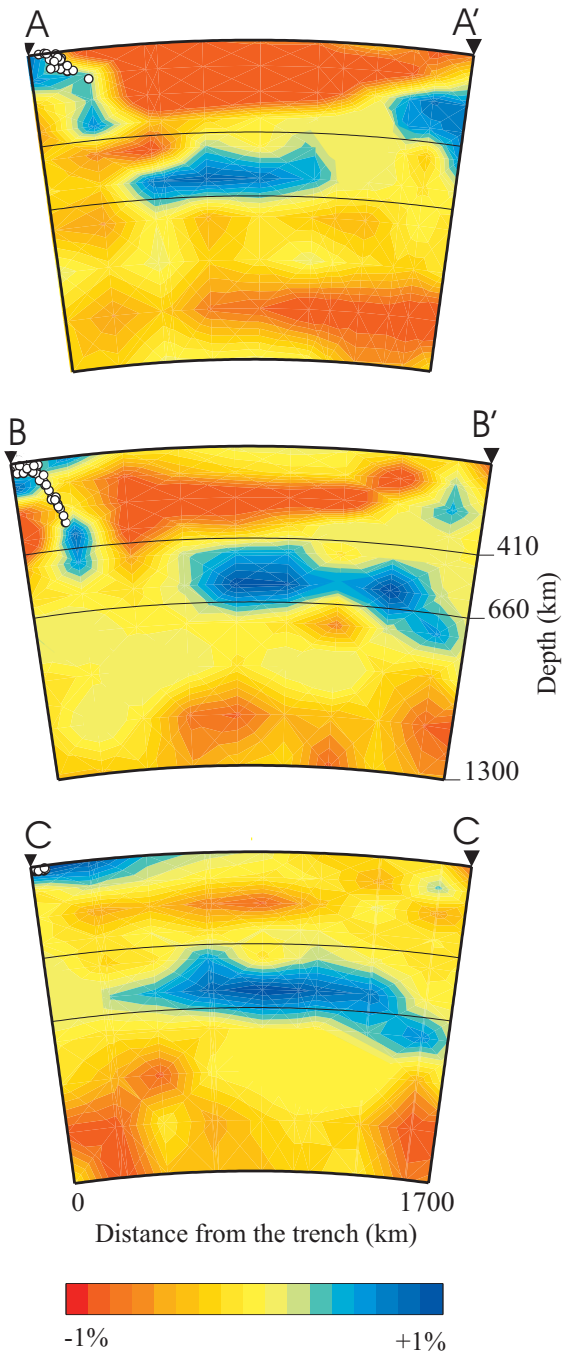

Figure 5. Cross-sections of the velocity anomalies along profiles in the Aleutian subduction zone. Their locations are shown in the Fig. 2. Red and blue denote slow and fast velocity anomalies, respectively, with a scale in per cent relative to the reference model ak135 (Kennett *et al.* 1995). Open circles represent the hypocentres of earthquakes of magnitudes ≥ 5.5.

from blocks with 1 per cent of perturbation relative to the ak135 earth model. This synthetic structure is stripped by zero perturbations in odd-numbered layers in order to investigate the vertical smearing. The restore resolution test is performed in the same way as the chequerboard resolution test. Figs 6 and 8 show the results of these additional tests, and indicate that the slab structures are in general well recovered and

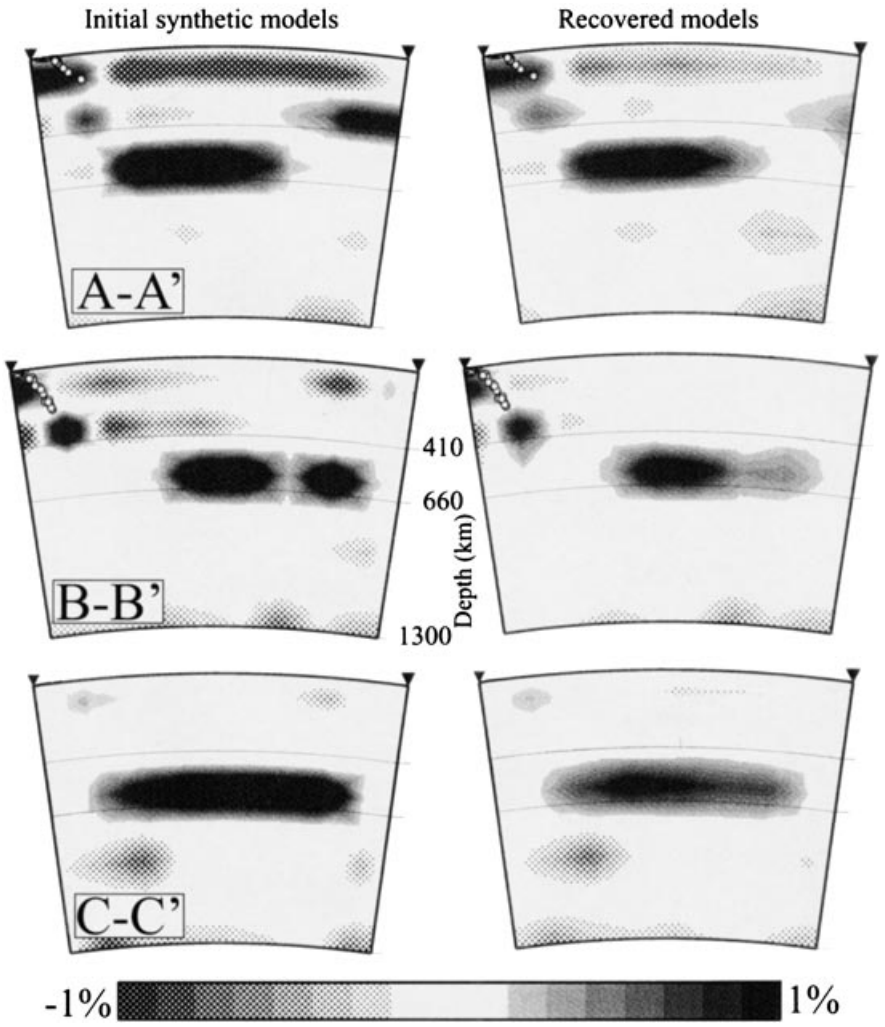

Figure 6. Results of the restore resolution test for the cross-sections given in Fig. 5. The hypothetical subducted slab is stripped by zero perturbations in odd-numbered layers in order to investigate the vertical smearing (left column). The corresponding recovered synthetic model is presented in the right column. The hypothetical slabs are constructed from blocks with 1 per cent of perturbation relative to the ak135 earth model (Kennett *et al.* 1995). The values of the velocity perturbations at each point of the cross-sections are linearly interpolated between neighbouring cells. The velocity perturbation scale in per cent relative to the ak135 Earth model is shown at the bottom.

that vertical smearing is observed mainly in the depth range shallower than $\sim$300 km near the active subduction zones.

The configuration of the high-velocity anomaly behind the northern-Kurile to Kamchatka arc is more complicated. Fig. 7 shows the cross-sections along profiles DD′, EE′ and FF′ across the Kamchatka arc (see Fig. 2 for locations), and Fig. 8 shows the corresponding results of the restore resolution test. The cross-section along DD′ gives us a typical image of the northern Kurile to souhern Kamchatca arc. The Wadati–Benioff zone extends down to the bottom of the upper mantle at 660 km depth. The high-velocity zone associated with this Wadati–Benioff zone extends further beyond its leading edge, kinks backwards against the subduction direction below the 660 km discontinuity, and reaches a depth of about 900 km, in qualitative agreement with the seismic image obtained by van der Hilst *et al.* (1991) for the northern Kurile arc. This high-velocity zone probably represents the subducted slab of the Pacific plate.

A gap opens and widens between the shallower and deeper parts of this subducted slab image to the northeast along the Kamchatka Peninsula. The shallower part is a high-velocity zone associated with the Wadati–Benioff zone which progressively shortens to the northeast. The deeper part gives a cross-sectional view of an isolated high-velocity body at depths near to and below the 660 km discontinuity. A comparison of the cross-sections along profiles DD′, EE′ and FF′ clearly shows this tendency. In the DD′ section (southern Kamchatka), the slab-like high-velocity zone is continuous from the Earth's surface to 900 km depth. In the EE′ section (central Kamchatka), there is a gap between the shallower and deeper parts of the high-velocity zone. The shallower part of the high-velocity zone coincides with but extends slightly beyond the Wadati–Benioff zone. The gap between the two high-velocity zones widens further to the northeast. To this end, as in the FF′ section (northern Kamchatka), the shallower part of the high-velocity zone associated with the Wadati–Benioff zone

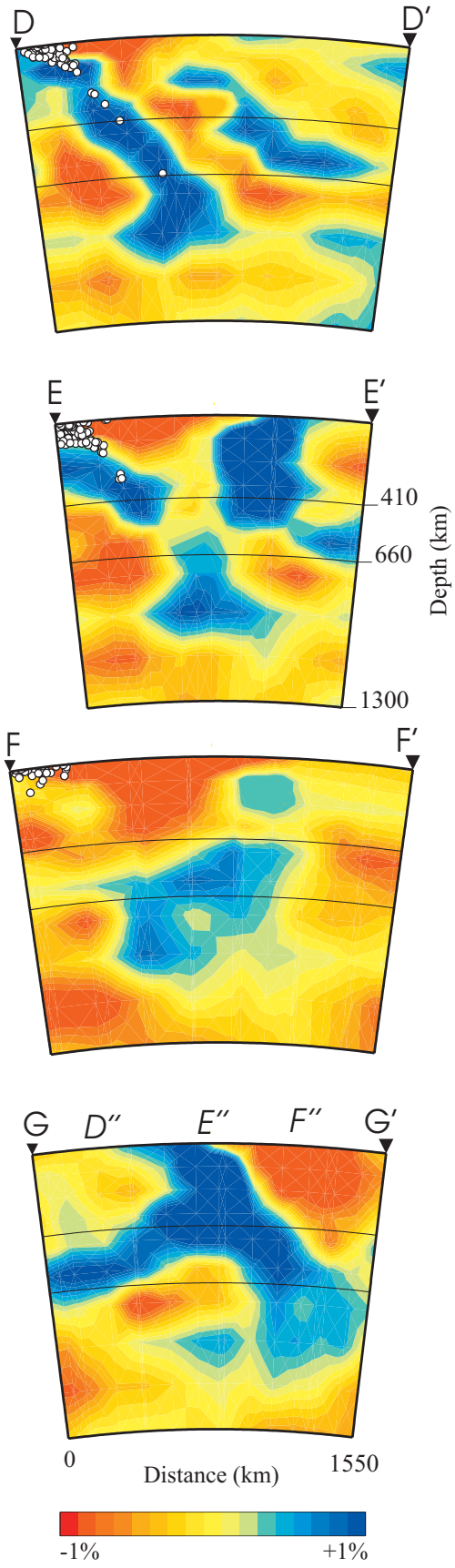

Figure 7. Cross-sections of the velocity anomalies along profiles in the Kurile–Kamchatka subduction zone. Their locations are given in Fig. 2. See Fig. 5 for further explanation.

becomes too short to be identified as an inclined slab. The deeper part of the high-velocity zone, on the other hand, still persists below the 660 km discontinuity.

The DD′, EE′ and FF′ cross-sections indicate the presence of another remarkable high-velocity zone behind the Kurile–Kamchatka arc, running subparallel to the presently subducting slab. In the DD′ section, this high-velocity zone dips to the northwest, extends from ∼200 km to ∼660 km depth, and spreads subhorizontally above the 660 km discontinuity. This high-velocity zone shallows to the northeast, and in the EE′ section it takes its shallowest position. Further northeastwards, the high-velocity zone begins to be located at greater depths. In the FF′ section it is located at depths below ∼400 km, reaching the 660 km discontinuity without a significant horizontal spread. Fig. 7 illustrates this backarc high-velocity zone, showing a cross-section along profile GG′ (see Fig. 2 for location), which traverses the three profiles DD′, EE′ and FF′ with intersections at D″, E″ and F″, respectively. This figure demonstrates clearly the presence of a vertically Λ-shaped high-velocity zone at the back of the Kamchatka arc, which is shallowest near E′ and deepens in the direction towards D′ to flatten above the 660 km discontinuity and also in the direction towards F″ to continue apparently southwards to the isolated deepest anomaly below the Wadati–Benioff zone. Bijwaard *et al.* (1998) pointed out the presence of a high-velocity zone in the Kamchatka backarc region, but its geometry was not resolved in detail.

5 DISCUSSION

For the Aleutian arc, we identified two high-velocity anomalies, one associated with the Wadati–Benioff zone and the other flattening above the 660 km discontinuity. The high-velocity anomaly associated with the Wadati–Benioff zone can be interpreted straightforwardly as representing the lithospheric slab subducted from the Aleutian trench. According to this interpretation, the subducted slab now reaches a depth somewhat greater than that of the leading edge of the Wadati–Benioff zone.

The Aleutian arc has a long history of normal subduction of the Kula plate, which was succeeded by ridge subduction at ∼48 Ma (Engebretson *et al.* 1985; Gordon & Jurdy 1986; Lonsdale 1988; Lithgow-Bertelloni & Richards 1998). This ridge subduction, after a transitory period of normal subduction, was followed by the oblique subduction of the Pacific plate which commenced when the Hawaiian–Emperor bend occurred (∼43 Ma; Gordon & Jurdy 1986). Since then, the convergence rate of the Pacific plate against the Aleutian arc has been small, and this small convergence rate is probably responsible for the relatively small length of slab subducted from the Aleutian trench, as seen in our tomographic model (Fig. 5). Based on this subduction history, we argue that the high-velocity anomaly horizontally spreading at depths of ∼600 km beneath the Bering Sea represents the relic of the subducted slab of the Kula plate. We also suggest that the remarkable gap between this remnant slab anomaly and the one associated with the Wadati–Benioff zone is diagnostic of the ridge subduction at ∼48 Ma (Fig. 9a).

For the northern Kurile to Kamchatka arcs we have distinguished two high-velocity anomalies, one associated with the Wadati–Benioff zone and the other vertically Λ-shaped behind the arc, although such a distinction is somewhat

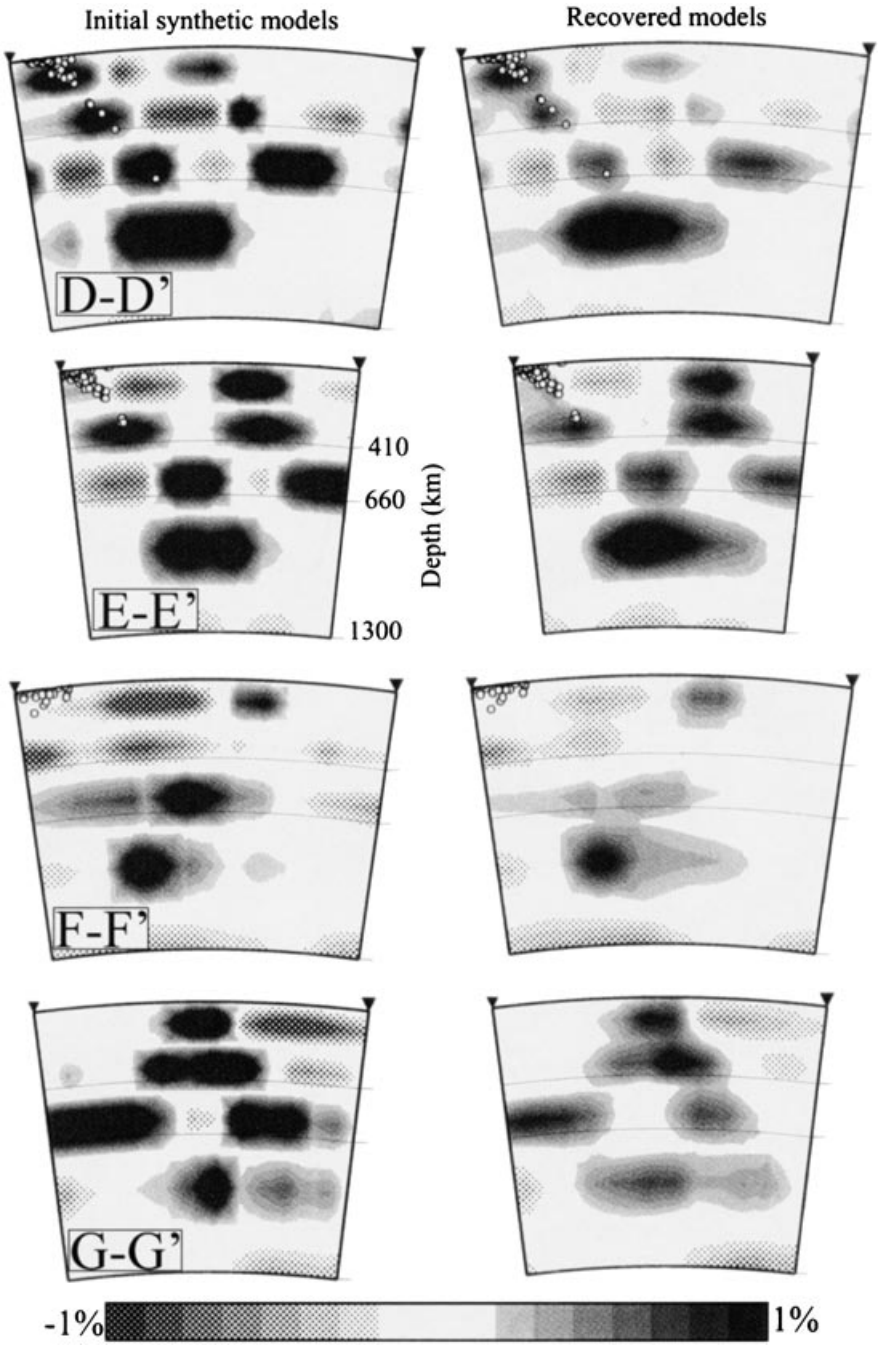

Figure 8. Results of the restore resolution test for the cross-sections given in Fig. 7. See Fig. 6 for further explanation. The vertical smearing is observed mainly near the trench for depths shallower than ~300 km.

subjective because it is based entirely on the apparent configuration of tomographic images. The high-velocity zone associated with the Wadati–Benioff zone can be directly related to the subducted slab from the Kurile trench. It is difficult, however, to explain why this subducted slab is separated into shallower and deeper parts with a gap increasing in a northeastward direction along the Kamchatka Peninsula. Watson & Fujita (1985) argued, based on geological evidence, that volcanism and convergence in the Kamchatka region ceased at about 55 Ma but resumed about 30 Myr ago. This resumption of convergence in Kamchatka appears to have been roughly synchronous with the opening of the Okhotsk Sea and retreat of the Kurile Trench, which continued through the Oligo–Middle Miocene epoch (Miyasaka *et al.* 1986; Kimura 1994). The cessation of convergence in Kamchatka at ~55 Ma appears to have been only slightly preceded by a jump in the subduction zone from the northeastern Asian margin to the Kurile–Kamchatka trench and the consequent trapping of the Okhotsk oceanic plate, which is estimated to have occurred in the period 55–65 Ma (Parfenov & Natal'in 1985; Kimura 1994).

We speculate that the high-velocity zone associated with the Wadati–Benioff zone represents the Pacific plate subducted from the Kurile trench, a process activated at ~55 Ma, and

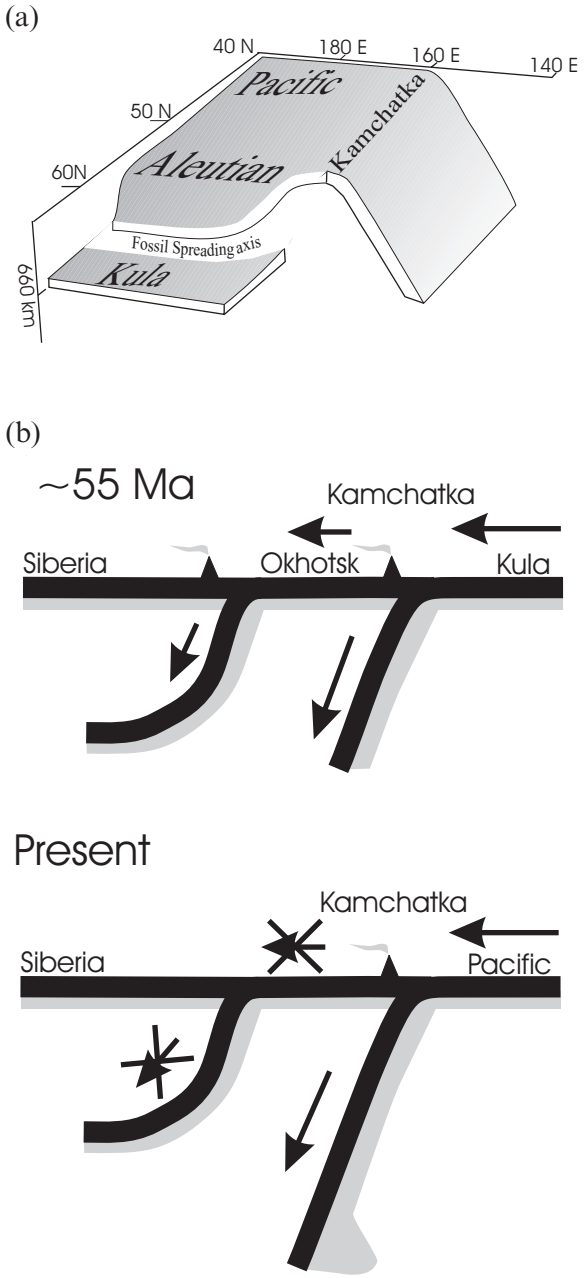

Figure 9. Schematic cartoons for the remnant subducted slabs below the (a) Bering and (b) Okhotsk seas. (a) The fossil spreading axis separates the remnant Kula plate from the present subducted Pacific plate below the Bering Sea. (b) The Okhotsk subduction zone was active before ~55 Ma, and activity ceased after accretion of the Kamchatka peninsula. The remnant Okhotsk plate can be seen beneath the fossil subduction zone at present.

that the Λ-shaped high-velocity zone behind it is the relic of the subducted part of the Okhotsk plate (Fig. 9b). We also argue that the resumption of subduction in the Kamchatka region at ~30 Ma started near its southern end and proceeded to the northeast, resulting in a northeastward shortening of the subducted part of the Pacific plate. In fact, according to Gordon & Jurdy (1986) and Bazhenov *et al.* (1991), the junction between the Aleutian and Kurile trenches was located near the southern end of the Kamchatka Peninsula until ~30 Ma, and then shifted to its present position in association with a clockwise rotation of the eastern Aleutian arc. The high-velocity body located below the 660 km discontinuity may then represent the slab material subducted from the Kurile trench before the cessation of convergence in the Kamchatka region.

A unique feature of the backarc high-velocity anomaly (Fig. 7) is a vertically Λ-shaped configuration as shown in the GG′ cross-section. This may indicate a contortion of the subducted slab of the Okhotsk plate. The Λ-shaped contortion of a subducted slab has been detected by deep seismicity and seismic tomography, for example at the junction between the Kurile and Honshu arcs (Miyamachi *et al.* 1994) and in the Molucca collision zone with the two opposing subducted slabs of the Molucca Sea plate (Widiyantoro & van der Hilst 1997).

6 CONCLUSIONS

A 3-D ray-tracing technique was successfully applied to the *P*-wave arrival time data reported by the GSR, ISC and NEIC in order to obtain the tomographic image of the area around the Kurile–Kamchatka and Aleutian arcs. Owing to the addition of a large number of GSR data, the *P*-wave tomographic images revealed high-velocity structures associated not only with the subducted slab of the Pacific plate but also with relicts of the subducted slabs below the Chukotka peninsula, and Okhotsk and Bering seas. The Pacific slab subducted from the Aleutian trench extends beyond the leading edge of the Wadati–Benioff zone. The broad high-velocity zone below the Bering Sea flattens above the 660 km mantle discontinuity. This subhorizontal high-velocity structure extends from ~60°N to ~70°N. Palaeotectonic reconstructions suggest that the high-velocity zone detected below the Bering Sea could be interpreted as a remnant slab of the Kula plate.

The Pacific slab subducted from the northern Kurile–southern Kamchatka trench extends to a depth of ~900 km, with a kink at depths below the 660 km discontinuity, and separates into shallower and deeper parts in central Kamchatka. The gap increases in a northeastward direction along the Kamchatka peninsula. The high-velocity zone subparallel to the subducted Pacific plate can be seen clearly below the Chukotka peninsula and Okhotsk Sea. This anomaly zone extends to depths of ~600 km and may be interpreted as a relict of the subducted Okhotsk plate. The subducted slab penetrates the lower mantle to a depth of ~800 km below the Chukotka peninsula, while it becomes subhorizontal in the mantle transition zone below the Okhotsk Sea.

ACKNOWLEDGMENTS

We thank B. L. N. Kennett and M. Obayashi for useful suggestions and discussions, and K. Koketsu and S. Sekine for their 3-D ray tracing code. J-J. Lévêque and an anonymous reviewer provided us with helpful comments and suggestions which improved the manuscript. We are also grateful to the staff of the Geophysical Survey of Russia, who helped us in data recompilation and digitization. AG and SW wish to thank the Japan Society for the Promotion of Science (JSPS) for a postdoctoral fellowship to conduct research at the Earthquake Research Institute, University of Tokyo. The GMT software package of Wessel & Smith (1995) was used in our study.

REFERENCES

Aki, K. & Lee, W.H.K., 1976. Determination of three-dimensional velocity anomalies under a seismic array using first P arrival times from local earthquakes, 1, A homogeneous initial model, *J. geophys. Res.,* **81,** 4381–4399.

Bazhenov, M.L., Burtman, V.S., Krezhovskih, O.A. & Shapiro, M.N., 1991. Paleotectonic reconstruction of the Aleutian arc: Kamchatka convergence zone, *Geotectonics,* **25,** 244–256.

Bijwaard, H., Spakman, W. & Engdahl, E.R., 1998. Closing the gap between regional and global travel-time tomography, *J. geophys. Res.,* **103,** 30 055–30 078.

Dziewonski, A.M., Hager, B.H. & O'Connell, R.J., 1977. Large-scale heterogeneities in the lower mantle, *J. geophys. Res.,* **82,** 239–255.

Engdahl, E.R. & Gubbins, D., 1987. Simultaneous travel time inversion for earthquake location and subduction zone structure in the central Aleutian islands, *J. geophys. Res.,* **92,** 13 855–13 862.

Engdahl, E.R., Van der Hilst, R.D. & Buland, R.P., 1998. Global teleseismic earthquake relocation with improved travel times and procedures for depth determination, *Bull. seism. Soc. Am.,* **88,** 722–743.

Engebretson, D.C., Cox, A. & Gordon, R.G., 1985. Relative motions between oceanic and continental plates in the Pacific basin, *Geol. Soc. Am., Spec. Paper*, 206.

Fukao, Y., Obayashi, M., Inoue, H. & Nenbai, M., 1992. Subducting slabs stagnant in the mantle transition zone, *J. geophys. Res.,* **97,** 4809–4822.

Gorbatov, A., Dominguez, J., Suarez, G., Kostoglodov, V., Zhao, D. & Gordeev, E., 1999. Tomographic imaging of the P-wave velocity structure beneath the Kamchatka peninsula, *Geophys. J. Int.,* **137,** 269–279.

Gordon, R.G. & Jurdy, D.M., 1986. Cenozoic global plate motions, *J. geophys. Res.,* **91,** 12 389–12 406.

Humphreys, E. & Clayton, R.W., 1988. Adaption of back projection tomography to seismic travel time problems, *J. geophys. Res.,* **93,** 1073–1085.

Inoue, H., Fukao, Y., Tanabe, K. & Ogata, Y., 1990. Whole mantle P-wave travel time tomography, *Phys. Earth planet. Inter.,* **59,** 294–328.

Kennett, B.L.N., Engdahl, E.R. & Buland, R., 1995. Constraints on seismic velocities in the Earth from travel-times, *Geophys. J. Int.,* **122,** 108–124.

Kimura, G., 1994. The latest Cretaceous—early Paleogene rapid growth of accretionary complex and exhumation of high pressure series metamorphic rocks in northwestern Pacific margin, *J. geophys. Res.,* **99,** 22 147–22 164.

Koketsu, K. & Sekine, S., 1998. Pseudo-bending method for three-dimensional seismic ray tracing in a spherical earth with discontinuities, *Geophys. J. Int.,* **132,** 339–346.

Lévêque, J.-J., Rivera, L. & Wittlinger, G., 1993. On the use of the checker-board test to assess the resolution of tomographic inversions, *Geophys. J. Int.,* **115,** 313–318.

Lithgow-Bertelloni, C. & Richards, M.A., 1998. The dynamic of Cenozoic and Mesozoic plate motions, *Rev. Geophys.,* **36,** 27–78.

Lonsdale, P., 1988. Paleogene history of the Kula plate: offshore evidence and onshore implications, *Geol. Soc. Am. Bull.,* **100,** 733–754.

Mikumo, T., Hirahara, K., Takeuchi, F., Wada, H., Tsukuda, T., Fujii, I. & Nishigami, K., 1995. Three-dimensional velocity structure of the upper crust in the Hida region, Central Honshu, Japan, and its relation to local seismicity, Quaternary active volcanoes and faults, *J. Phys. Earth,* **43,** 59–78.

Miyasaka, S., Hoyanagi, K., Watanabe, Y. & Matsui, M., 1986. Late Cenozoic mountain-building history in central Hokkaido deduced from the composition of conglomerate (in Japanese), *Monogr. Assoc. Geol. Collab. Jpn,* **31,** 285–294.

Miyamachi, H., Kasahara, M., Suzuki, S., Tanaka, K. & Hasegawa, A., 1994. Seismic velocity structure in the crust and upper mantle beneath northern Japan, *J. Phys. Earth,* **42,** 269–301.

Nolet, G., 1990. Seismic wave propagation and seismic tomography, in *Seismic Tomography,* pp. 1–23, ed. Nolet, G., Reidel, Norwell, MA.

Page, C.C. & Saunders, M.A., 1982. LSQR: an algorithm for sparse linear equations and sparse least squares, *ACM Trans. Math. Soft.,* **8,** 43–71.

Parfenov, L.M. & Natal'in, B.A., 1985. Mesozoic accretion and collision tectonics of northeastern Asia, in *Tectonostratigraphic Terranes of the Circum-Pacific Region,* pp. 363–373, ed. Howell, D.G., Circum-Pacific Council, Houston, TX.

Spakman, W. & Nolet, G., 1988. Imaging algorithms, accuracy and resolution in delay time tomography, in *Mathematical Geophysics,* pp. 155–187, ed. Vlaar, N.J., Reidel, Norwell, MA.

Thurber, C.H., 1983. Earthquake locations and three-dimensional crustal structure in the Coyote Lake area, central California, *J. geophys. Res.,* **88,** 8226–8236.

van der Hilst, R.D., Engdahl, E.R., Spakman, W. & Nolet, G., 1991. Tomographic imaging of subducted lithosphere below northwest Pacific island arcs, *Nature,* **353,** 37–43.

van der Hilst, R.D., Engdahl, E.R. & Spakman, W., 1993. Tomographic inversion of P and pP data for aspherical mantle structure below the northwest Pacific region, *Geophys. J. Int.,* **115,** 264–302.

van der Hilst, R.D., Widiyantoro, S. & Engdahl, E.R., 1997. Evidence for deep mantle circulation from global tomography, *Nature,* **386,** 578–584.

Watson, B.F. & Fujita, K., 1985. Tectonic evolution of Kamchatka and Sea of Okhotsk and implications for the pacific basin, in *Tectonostratigraphic Terranes of the Circum-Pacific Region,* pp. 333–348, ed. Howell, D.G., Circum-Pacific Council, Houston, TX.

Wessel, P. & Smith, W.H.F., 1995. New, Version of the Generic Mapping Tools released, *EOS, Trans. Am. geophys. Un.,* **76,** 329.

Widiyantoro, S., 1997. Studies of seismic tomography on regional and global scale, *PhD thesis,* Aust. Natl. University, Canberra.

Widiyantoro, S. & van der Hilst, R.D., 1997. Mantle structure beneath Indonesia inferred from high-resolution tomographic imaging, *Geophys. J. Int.,* **130,** 167–182.

Zhao, D., Hasegawa, A. & Horiuchi, S., 1992. Tomographic imaging of P and S wave velocity structure beneath northeastern Japan, *J. geophys. Res.,* **97,** 19 909–19 928.

Zhou, H. & Clayton, R.W., 1990. P and S wave travel-time inversions for subducting slab under the island arcs of the northwest Pacific, *J. geophys. Res.,* **95,** 6829–6851.